NeuroImage 226 (2021) 117588

Contents lists available at ScienceDirect

NeuroImage

journal homepage: www.elsevier.com/locate/neuroimage

Dynamic whole-brain metabolic connectivity during vestibular compensation in the rat

Maximilian Grosch[a,*], Magdalena Lindner[a,b], Peter Bartenstein[b,e], Thomas Brandt[a,c], Marianne Dieterich[a,d,e], Sibylle Ziegler[b], Andreas Zwergal[a,d]

[a] German Center for Vertigo and Balance Disorders, University Hospital of Munich, LMU Munich, Munich, Germany
[b] Department of Nuclear Medicine, University Hospital of Munich, LMU Munich, Munich, Germany
[c] Clinical Neurosciences, University Hospital of Munich, LMU Munich, Munich, Germany
[d] Department of Neurology, University Hospital of Munich, LMU Munich, Munich, Germany
[e] Munich Cluster of Systems Neurology, SyNergy, Munich, Germany

ARTICLE INFO

Keywords:
Vestibular compensation
Positron emission tomography
Metabolic connectivity
Graph theory
Acute vestibular syndrome

ABSTRACT

Unilateral damage to the inner ear results in an acute vestibular syndrome, which is compensated within days to weeks due to adaptive cerebral plasticity. This process, called central vestibular compensation (VC), involves a wide range of functional and structural mechanisms at the cellular and network level. The short-term dynamics of whole-brain functional network recruitment and recalibration during VC has not been depicted *in vivo*. The purpose of this study was to investigate the interplay of separate and distinct brain regions and *in vivo* networks in the course of VC by sequential [^{18}F]-FDG-PET-based statistical and graph theoretical analysis with the aim of revealing the metabolic connectome before and 1, 3, 7, and 15 days post unilateral labyrinthectomy (UL) in the rat. Temporal changes in metabolic brain connectivity were determined by Pearson's correlation ($|r| > 0.5$, $p < 0.001$) of regional cerebral glucose metabolism (rCGM) in 57 segmented brain regions. Metabolic connectivity analysis was compared to univariate voxel-wise statistical analysis of rCGM over time and to behavioral scores of static and dynamic sensorimotor recovery. Univariate statistical analysis revealed an ipsilesional relative rCGM decrease (compared to baseline) and a contralesional rCGM increase in vestibular and limbic networks and an increase in bilateral cerebellar and sensorimotor networks. Quantitative analysis of the metabolic connections showed a maximal increase from baseline to day 3 post UL (interhemispheric: 2-fold, ipsilesional: 3-fold, contralesional: 12-fold) and a gradual decline until day 15 post UL, which paralleled the dynamics of vestibular symptoms. In graph theoretical analysis, an increase in connectivity occurred especially within brain regions associated with brainstem-cerebellar and thalamocortical vestibular networks and cortical sensorimotor networks. At the symptom peak (day 3 post UL), brain networks were found to be organized in large ensembles of distinct and highly connected hubs of brain regions, which separated again with progressing VC. Thus, we found rapid changes in network organization at the subcortical and cortical level and in both hemispheres, which may indicate an initial functional substitution of vestibular loss and subsequent recalibration and reorganization of sensorimotor networks during VC.

Introduction

Ablation of one inner ear in the rat causes an acute vestibular syndrome, which includes spontaneous nystagmus, head and body tilt, posturing, barrel rolling and circular walking. Remarkably, the initial symptoms of vestibular asymmetry rapidly improve over days to weeks by means of a process called central vestibular compensation (Curthoys and Halmagyi, 1995; Dieringer, 1995; Dutia, 2010). This includes initial functional substitution and recalibration and long-term structural restoration of the vestibular tone imbalance due to the lack of vestibular input. Vestibular compensation is achieved by a dynamic cascade of cerebral plasticity mechanisms, which take place at both the cellular and the brain network level (Straka et al., 2005; Tighilet and Chabbert, 2019; Zwergal et al., 2016). In the past, the majority of studies focused on the cellular level of plasticity mostly in the vestibular nuclei (Beraneck et al., 2003; Dutheil et al., 2009; Kaufman et al., 1992; Ris et al., 1995; Shao et al., 2012; Smith and Curthoys, 1988; Tighilet and Chabbert, 2019). Changes of intrinsic membrane properties, receptor expression and neurotransmission, reactive neurogenesis and glial activation were described as cellular substrates of vestibular compensation (Bergquist et al., 2008; Cameron and Dutia, 1997; de Waele et al., 1995; Lim et al., 2010; Shao et al., 2012; Tighilet and Chabbert, 2019; Vibert et al., 2000; Yamanaka et al., 2000; Zwergal et al., 2017). Less is known about the dynamic changes of the

* Corresponding author.
E-mail address: maximilian.grosch@med.uni-muenchen.de (M. Grosch).

https://doi.org/10.1016/j.neuroimage.2020.117588
Received 26 August 2020; Received in revised form 5 November 2020; Accepted 19 November 2020
Available online 26 November 2020

various functional brain network interactions in the course of recovery, although it is well known that the vestibular system is closely connected to other sensorimotor and cognitive networks at various subcortical and cortical levels (Brandt and Dieterich, 2017; Leong et al., 2019; Rancz et al., 2015).

Novel imaging techniques allow functional and metabolic network connectivity within the whole-brain to be depicted (Straathof et al., 2019; Yakushev et al., 2017). The majority of brain connectivity studies were performed using functional magnetic resonance imaging (fMRI). Recently, metabolic connectivity analysis, based on fluorodeoxyglucose ([^{18}F]-FDG) positron emission tomography (PET), has been applied more frequently in preclinical and clinical neuroimaging studies (Yakushev et al., 2017). In the current study, serial [^{18}F]-FDG-PET images were acquired in rats prior and up to 15 days after unilateral labyrinthectomy (UL) and analyzed for dynamic changes of whole-brain metabolic connectivity using state-of-the-art graph theoretical measures (Sanabria-Diaz et al., 2013). We aimed to investigate the applicability of [^{18}F]-FDG-PET-based brain connectivity methods to disclose temporal changes of functional networks during vestibular compensation. It was hypothesized that the interaction of vestibular networks with sensory, motor, and cognitive networks would first increase after the UL, and gradually normalize over the course of behavioral recovery. Overall, the study envisions establishing a more complete view of the rearrangement and recruitment of various functional networks initiated by a peripheral unilateral vestibular lesion.

Methods

Animals

All animal experiments were approved by the government of Upper Bavaria and performed in accordance with the guidelines for the use of living animals in scientific studies and the German Law for the Protection of Animals. Male Sprague-Dawley rats (mean 400 ± 20 g, age 3 months at time of UL, Charles River Ltd, UK) were housed two animals per cage in a temperature- and humidity-controlled room with a 12 h light/dark cycle, with free access to food and water. The animals were recruited from two previous studies (Lindner et al., 2017; Lindner et al., 2019), which were conducted with the same protocol regarding experimental environment, animal handling, evaluated parameters, and longitudinal measurement timeline. After excluding erroneous images from the dataset due to artifacts or incorrect tracer application, a constant number of 17 animals per day in total were included in the current study.

Experimental procedure

In all animals, a left-sided unilateral labyrinthectomy (UL) was performed by injection of bupivacaine and p-arsanilic acid to induce an acute vestibular syndrome. All animals underwent behavioral testing by clinical scoring of vestibular imbalance and instrumental analysis of locomotion before and on days 1, 3, 7, and 15 after UL (Fig. 1a). Sequential [^{18}F]-FDG-PET images of the subjects were acquired prior to and 1, 3, 7, and 15 days post UL (Fig. 1b). After preprocessing the images (i.e., cropping, registration, segmentation) (Fig. 1c,d), univariate analysis was used to depict changes of regional [^{18}F]-FDG uptake as a measure of cerebral glucose metabolism per region over time. Next, population-based connectivity analysis was performed to investigate sequential changes of the whole-brain metabolic connectome. Therefore, Pearson's correlations between segmented brain regions were calculated and used to determine interregional connections.

Chemical unilateral labyrinthectomy

Chemical UL was performed as described earlier (Anniko and Wersall, 1977; Beck et al., 2014; Magnusson et al., 2002; Vignaux et al., 2012; Zwergal et al., 2017): Animals were anesthetized with 1.5% isoflurane in O_2 delivered up to 1.2 l/min O_2 via a mask. For surgical analgesia, 1.5 mg/kg meloxicam was injected s.c. before and 3 days after surgery. An additional 5 ml saline was injected s.c. as a bolus. After local anesthesia with 1% bupivacaine hydrochloride, a left paramedian incision was made to expose the lamboidal ridge and the external ear canal. The external ear canal was opened just anterior to the exit point of the facial nerve. With a 26-gauge needle the tympanic membrane was perforated caudally to the hammer shaft, and about 0.150 ml of a 20% bupivacaine solution was instilled into the tympanic cavity. For about 2 min the bupivacaine solution was aspirated and instilled slowly again multiple times. The same procedure was followed to instill 0.150 ml of a 10% solution of p-arsanilic acid, which irreversibly desensitized the primary sensory cells of the inner ear (Vignaux et al., 2012). After the last thorough aspiration, the wound was closed by skin suture and for preventive antibiosis 2 mg/kg marbofloxacin was injected s.c. for 3 days.

Clinical scoring of vestibular asymmetry after UL

Behavioral symptoms of vestibular imbalance were scored by experienced veterinarians for four components after unilateral vestibular ablation (based on Bergquist et al., 2008): nystagmus, postural asymmetry, head roll tilt, and elevation tail test. Each component was given a score of up to 10:

- *Nystagmus* was observed visually. Intensity of spontaneous nystagmus was scored with 6–10 points, with 1 point for every 60 beats per minute (bpm). In the absence of spontaneous nystagmus at rest, the animal was touched gently. If nystagmus was evoked, it was scored with 1–5 points, with 1 point for every 60 bpm.
- *Postural deficits* were scored as follows: spontaneous barrel rolling - 10 points; barrel rolling evoked by light touch or air-puff - 9 points; recumbent position on lesion side without leg support - 8 points; some ipsilesional leg support - 7 points; moving around on one side or using ipsilesional legs for recumbent support - 6 points; moving around with bilateral leg support - 5 points; moving around with occasional falls to the ipsilesional side - 4 points; moving around leaning towards the ipsilesional side - 3 points; hardly noticeable asymmetry - 2 points; postural asymmetry only noticeable when picked up - 1 point.
- Spontaneous *head roll tilt* was scored by estimating the angle between the jaw plane and the horizontal, with 10 points given either for a 90° (deg) angle or if the animal rested recumbent on the lesion side or showed barrel-rolling towards that side. 7 points correlated with a 60 deg and 5 points with a 45 deg angle.
- Influence of perceptive somatosensory input on postural control during VC was examined by the *elevation tail test* (ETT). Animals were picked up from the ground at the radix of their tail and body rotation was scored by estimating in degrees, with 10 points given for more than 360 deg, 8 points for 180-360 deg, 6 points for less than 180 deg and 0 points for no relevant rotation.

Instrumental locomotor analysis

Testing of locomotor behavior was performed in an open field using automated video tracking (EthoVision System, Noldus, Netherlands). Animals were allowed to move freely in the quadratic open field (side length 70 cm) for 10 min. Position of nose, body center, and tail were automatically detected by video software. Mean locomotor velocity and cumulative duration of movement were quantified. Locomotor velocity was taken as an overall estimate of mobility, as suggested by previous studies (Lindner et al., 2019; Rastoldo et al., 2020).

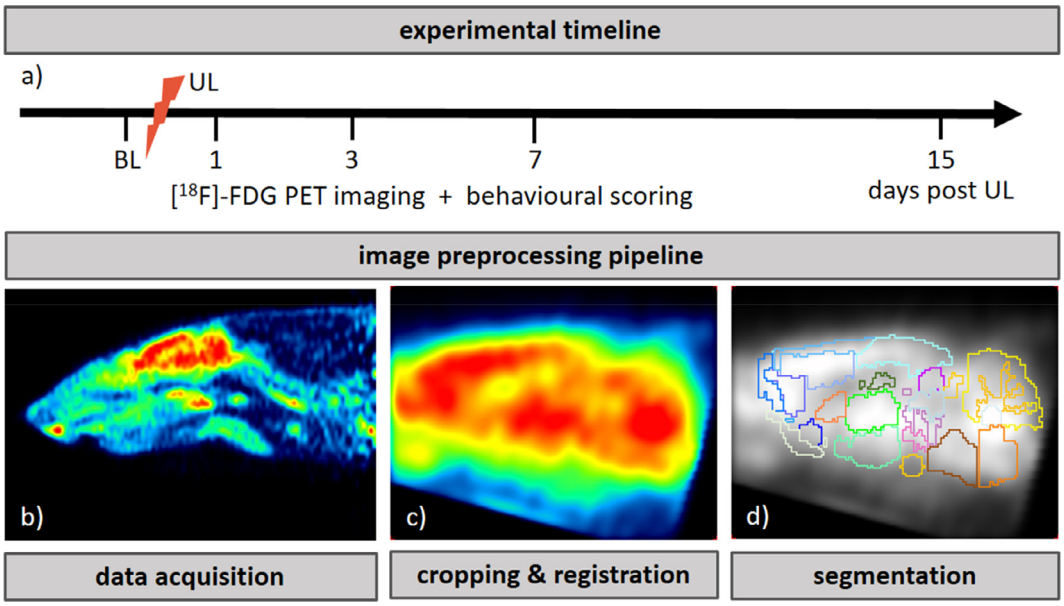

Fig. 1. Experimental protocol. a) Behavioral scoring and [^{18}F]-FDG PET imaging were conducted before and on days 1, 3, 7, and 15 post UL in 17 rats in total; b-d) Images were acquired, reconstructed, cropped, registered, filtered, normalized, and segmented prior to analysis. BL: baseline, [^{18}F]-FDG: [^{18}F]-Fluorodeoxyglucose, PET: positron emission tomography, UL: unilateral labyrinthectomy.

PET imaging

Anesthesia was induced with isoflurane (as described above) and a cannula was placed in a lateral tail vein for [^{18}F]-FDG bolus injection (in 0.5 ml saline). Then, the animals were awakened and were allowed to move freely for an uptake period of 30 min until anesthesia was induced again with isoflurane (1.8%) for the PET-scan. Two animals per scan were positioned in the Siemens Inveon PET scanner (Siemens Healthineers, Erlangen, Germany) and were kept warm with a heating pad. In order to avoid head movement, the head position was fixed using a custom-made head-holder. Emission data were recorded for 30 min followed by a 7-min transmission scan using a rotating [^{57}Co] point source. Upon recovery from anesthesia, the rats were returned to their home cages (Beck et al., 2014; Lindner et al., 2019).

Image processing & statistical analysis

Emission recordings were reconstructed using an Ordered Subsets Expectation Maximization (OSEM-3D) algorithm with scatter and attenuation correction (Siemens Healthineers, Erlangen, Germany) yielding a 128 × 128 × 159 image matrix (Fig. 1b). For attenuation correction, the corresponding transmission measurement at the end of the emission scan was used. The voxel dimensions of the reconstructed images were 0.78 × 0.78 × 0.80 mm^3 (Zwergal et al., 2016). Radioactivity distribution in the reconstructed images was used as a surrogate of the regional cerebral glucose metabolism (rCGM). Cropping and a template-based rigid coregistration into Px Rat (W. Schiffer) atlas space was performed (Schiffer et al., 2006) using PMOD medical image analysis software (PMOD Technologies LLC, RRID: SCR_016547, v4.004) (Fig. 1c). An isotropic Gaussian filter with 0.8 mm FWHM and whole-brain normalization was applied in order to achieve comparability between all images. Images were segmented into 57 brain regions using W.Schiffer's rat brain atlas (Fig. 1d). The *brain blood flow* region depicts a brain vessel and was therefore not included for further processing. Mean normalized activity values were extracted for each brain region using PyRadiomics (Van Griethuysen et al., 2017) Python package (Fig. 2a).

To evaluate the quality of the dataset, the functionality of the processing pipeline and the reasonability of brain connectivity analysis in vestibular disorders, univariate analysis was conducted and the results were compared to the expected outcome according to the literature (Zwergal et al., 2016). For univariate analysis, rCGM values in brain regions on days 1, 3, 7 and 15 post UL were compared voxel-wise to baseline using t-tests in SPM software (Wellcome Department of Cognitive Neurology, Great Britain) and the resulting t statistics were normalized yielding z-value images. The mean z-value was calculated for each brain region according to the corresponding voxels (Fig. 2b).

Metabolic brain connectivity

Metabolic brain connectivity analysis can be tackled with various approaches (Yakushev et al., 2017). In this work, normalized mean uptake values in segmented brain regions were correlated pairwise by Pearson's correlation and depicted as a confusion matrix as reported in the literature (Fig. 2c) (Sanabria-Diaz et al., 2013). Correlations with a threshold of $|r| > 0.5$ and $p < 0.001$ were considered as connections between the corresponding brain regions. The correlation matrix is a lower triangular matrix as connections are not directed and the main diagonal elements are zero due to excluded self-connections (Fig. 2c–d). The number of connections per brain hemisphere and between brain hemispheres was quantified. For visualization of hubs and connections, the centers of brain regions were projected into 2D planes of a 3D MRI cryoatlas template and connections were indicated as solid lines. For the purpose of clarity, brain regions were assigned to functional brain networks as described in appendix A (e.g., vestibular, other sensory, motor, hippocampal networks). Connections within functional networks were coded in unique colors and connections between different functional networks in white (Fig. 2e).

Furthermore, graph theoretical structures were created using NetworkX Python package (Hagberg et al., 2008) based on the correlation data and used for analysis of independent connected networks. Graphs are mathematical objects consisting of nodes and edges, where edges serve as links between the nodes. The degree of a node is the number of edges linking to other nodes. In this context, nodes represent brain regions and edges the determined connections. Thus, the correlation data was compiled into graph networks providing distinct mathematical properties. The center nodes were calculated for all networks, where the center nodes of a network are the nodes with a minimized maximal distance to other nodes. A rich-club analysis was performed to indicate

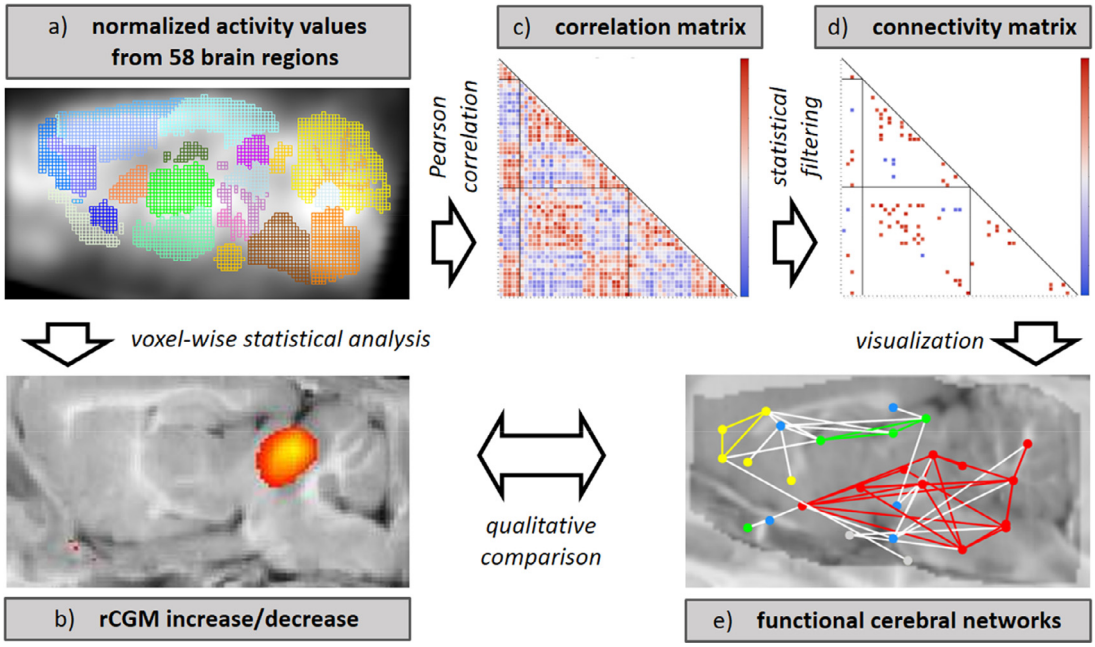

Fig. 2. [^{18}F]-FDG PET image processing and statistical analysis. a) Normalized activity values for 57 brain regions were extracted using PyRadiomics Python package. b) A univariate voxel-wise analysis was performed to depict relative changes of rCGM on days 1, 3, 7, and 15 post UL compared to baseline level. c) Pearson's correlations between all segmented brain regions were performed and d) statistically filtered to depict the metabolic connectome before and 1, 3, 7, and 15 days post UL. e) Metabolic connections were arranged by functional networks (including vestibular, other sensory, motor, cognitive networks) and visualized by projection into 2D planes of a 3D MRI cryoatlas template. Univariate and network analysis were compared qualitatively post hoc. rCGM: regional cerebral glucose metabolism.

hubs with the highest metabolic connectivity within the connected network. The corresponding rich-club consists of the brain regions with a degree greater than or equal to k, where k is the highest available degree in each subnetwork (Griffa and Van den Heuvel, 2018).

Statistics

Behavioral scoring parameters (nystagmus, postural asymmetry, head roll tilt, velocity in open field, movement duration) were statistically evaluated by ANOVA with Bonferroni post-hoc testing using Python statistics package.

Data availability

Data and code reported in this article will be shared with any appropriately qualified investigator on request.

Results

Behavioral analysis

After UL, animals showed severe signs of vestibular imbalance including spontaneous nystagmus, postural asymmetry, head roll tilt and body turns on elevated tail rotation test. Nystagmus peaked on day 1 post UL (8.8 ± 0.8) and steadily improved until it disappeared on day 15 post UL (ANOVA: F-value: 156.2, $p < 0.0001$). Post hoc tests indicated a significant decrease of nystagmus on days 7 and 15 compared to days 1 and 3 ($p < 0.0001$, respectively) (Fig. 3a). The intensity of head roll tilt was maximal on day 3 post UL (9.8 ± 0.7) and significantly improved until day 15 post UL (7.1 ± 1.6) (ANOVA: F-value: 206.2, $p < 0.0001$, post hoc comparison days 3 and 15: $p < 0.0001$) (Fig. 3b). Postural asymmetry increased until reaching a maximum on day 3 post UL (8.7 ± 0.8) and subsequently decreased until day 15 post UL (3.4 ± 2.3) (ANOVA: F-value: 107.1, $p < 0$ .0001, post hoc comparison days 3 and 15: $p < 0.0001$) (Fig. 3c). Elevation tail test symptoms revealed the highest score of 10.0 ± 0.0 on day 3 post UL and improved significantly to 8.9 ± 1.4 on day 15 post UL (post hoc comparison: $p = 0.003$) (Fig. 3d). The movement duration in the open field at baseline was 313.3 ± 36.9 s and dropped to 127.7 ± 75.3 s on day 1 post UL. Thereafter, movement duration increased significantly to 419.5 ± 64.7 s on day 15 post UL (Fig. 3e) (ANOVA: F-value: 26.2, $p < 0.0001$, post hoc comparison baseline, days 1, 3 to day 15: $p < 0.001$, respectively). The mean locomotor velocity decreased from a baseline level of 6.2 ± 1.4 cm/s to a minimum of 1.6 ± 1.1 cm/s on day 1 post UL, and from then increased steadily to 13.2 ± 4.3 cm/s on day 15 post UL (ANOVA: F-value: 27.2, $p < 0.0001$, post hoc comparison baseline, days 1, 3 to day 15: $p < 0.01$, respectively) (Fig. 3f).

z-score image analysis

For days 1, 3, 7, and 15 post UL, the relative increase and decrease of rCGM (compared to baseline) was determined in 57 segmented brain regions as normalized z-scores (representing the significance of t-statistics in unit standard deviation). For the sake of presentation, brain regions were grouped into the functional domains (cerebellar, midbrain, audiovestibular, sensorimotor, limbic, retrosplenial, parietal). The following regions consistently showed a relative decrease of rCGM until day 15 post UL: ipsilesional midbrain (including colliculus inferior, superior), ipsilesional audiovestibular cortex (including insula, auditory cortex), ipsilesional visual cortex, ipsilesional hippocampal formation (including entorhinal cortex, anterior, posterior hippocampus) (Fig. 4). In contrast, the following regions had a higher relative rCGM up to day 15 post UL: bilateral cerebellum (including gray and white matter), contralesional midbrain, contralesional visual cortex, bilateral somatosensory and motor cortex, bilateral retrosplenial and parietal cortex, contralesional hippocampal formation (including entorhinal cortex). The right amygdala had an increased rCGM on days 1 and 3 compared to baseline, while the left amygdala by trend had a decreased rCGM (Fig. 4).

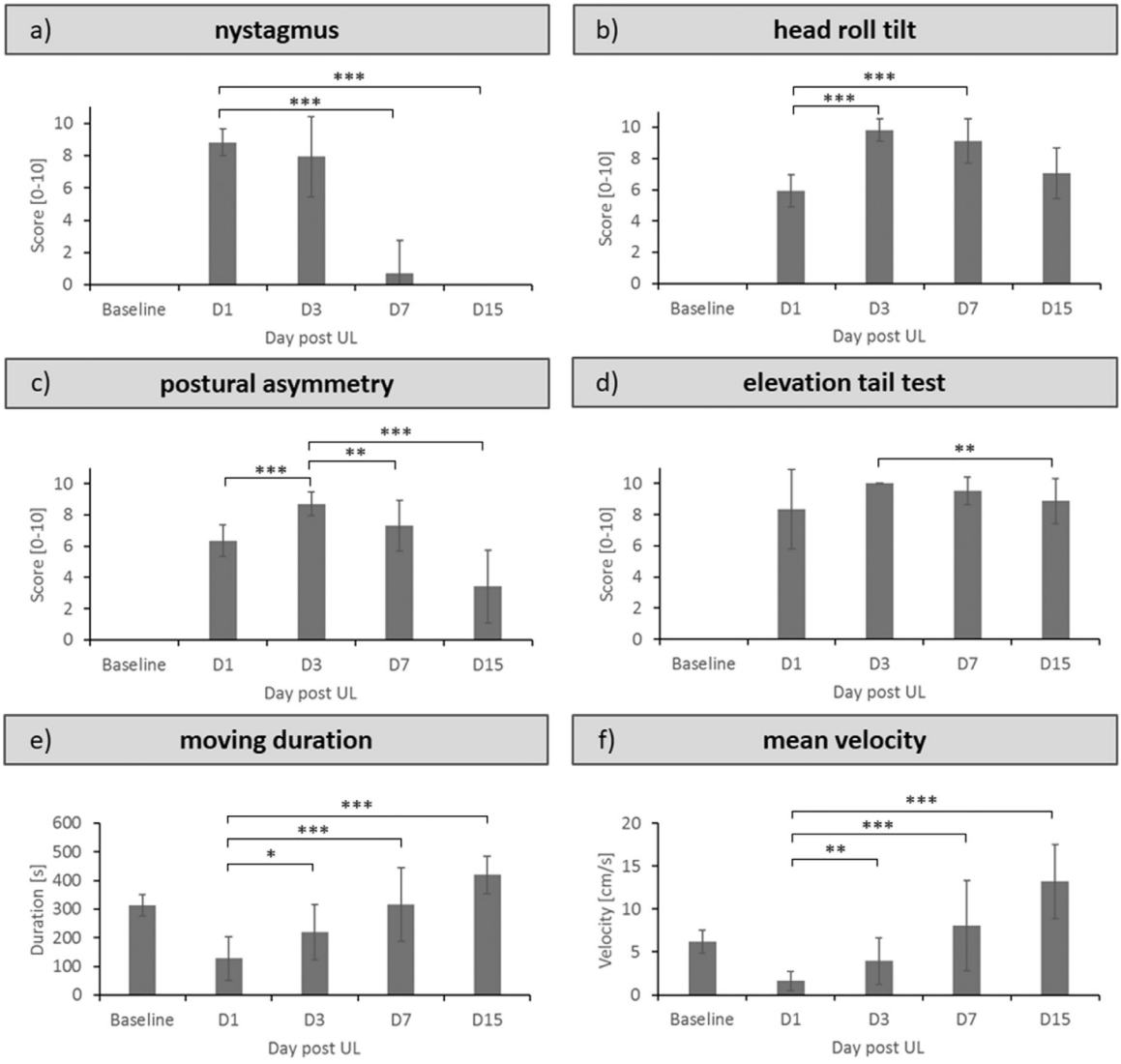

Fig. 3. Clinical scoring parameters of vestibular asymmetry and quantitative assessment of locomotion. Nystagmus (a), head roll tilt (b), postural asymmetry (c), and elevation tail test (d) were evaluated by experienced veterinarians on 0–10 scale. Duration of movement (e) and mean velocity (f) were measured during a 10 min stay in the open field. Values are depicted as mean ± standard deviation. Significant changes of scores (a–d) are depicted relative to the maximum score, significant changes of open field parameters (e,f) relative to the minimum value (* $p < 0.01$, ** $p < 0.005$, *** $p < 0.001$). Significant difference to baseline levels are not illustrated for sake of clarity. D: day, UL: unilateral labyrinthectomy.

Quantification of metabolic connectivity

The total number of significant connections (defined by Pearson's correlations with a threshold of $|r| > 0.5$ and $p < 0.001$) was minimal at baseline, increased up to a maximum on day 3 post UL, and decreased again until day 15 post UL to a level above baseline (Fig. 5). Thus the dynamic of relevant connections resemble the clinical course of vestibular compensation. Generally, positive correlations were more frequent than negative correlations. Looking at connections between and within hemispheres, the increase of connections until day 3 post UL was mostly due to more interhemispheric (i.e., left-right) connections (baseline: 16, day 1: 25, day 3: 36), and connections in the contralesional (i.e., right) hemisphere (baseline: 2, day 1: 19, day 3: 29). Connections in the ipsilesional (i.e., left) hemisphere increased only moderately (baseline: 4, day 1: 9, day 3: 13). An asymmetry in the number of connections between the contra- and ipsilesional hemisphere remained until day 7 post UL (15 vs. 7), while on day 15 post UL the pattern became more symmetrical (15 vs. 13) (Fig. 5).

Changes of metabolic connectivity during vestibular compensation

For the sake of clarity, the significant metabolic connections were grouped into the following functional networks: vestibular network (including medulla, cerebellum, midbrain, thalamus, insula), other sensory networks (including visual, somatosensory, auditory cortex, olfactory bulb), motor executive networks (including primary motor cortex, frontal cortex, basal ganglia), limbic networks (including amygdala, entorhinal cortex, anterior, posterior hippocampus, retrosplenial cortex) (Supplementary table 1). Connectivity within and between networks was visualized by 2D projection of connections on to a 3D cryoatlas MRI template (Fig. 6). At baseline, the vestibular networks were mostly connected at the brainstem-cerebellar level. On days 1 and 3 post UL, connectivity along ascending vestibular projections to the thalamus and cortex, as well as within thalamo-cortical networks increased massively with a preponderance to the contralesional hemisphere. Vestibular metabolic connectivity shifted back to brainstem-cerebellar networks until day 15 post UL. Metabolic connectivity in multisensensory (visual,

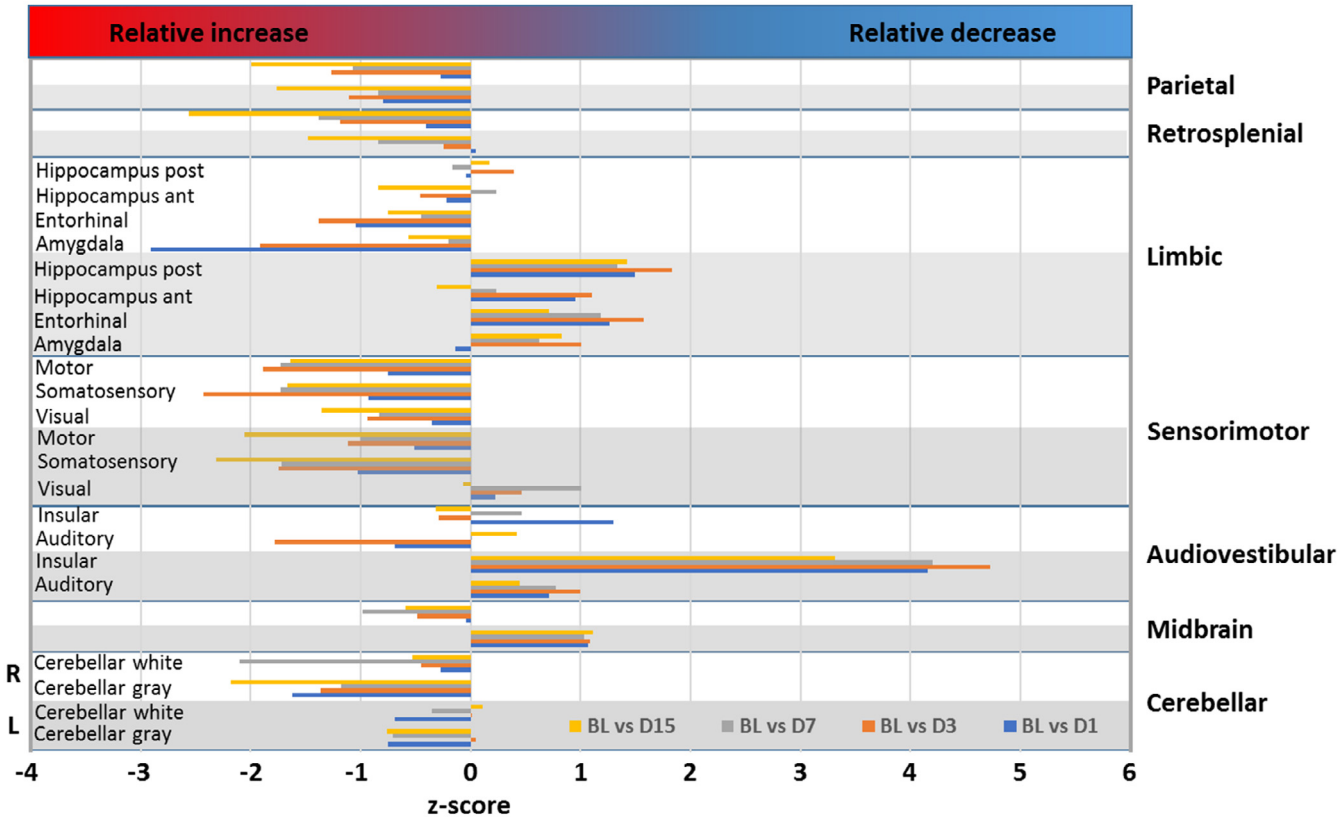

Fig. 4. Results of the univariate analysis in different brain regions during vestibular compensation. The regions are grouped by functional networks (cerebellar, midbrain, audiovestibular, sensorimotor, limbic, retrosplenial, parietal) and depicted for left-sided (L), i.e., ipsilesional regions (gray) and right-sided (R), i.e., contralesional regions (white) for the sake of clarity. Days post UL are color-coded (blue: day 1, orange: day 3, gray: day 7, yellow: day 15). The relative increase and decrease of regional cerebral glucose metabolism (rCGM) is expressed as normalized z-scores derived from SPM analysis. Relative rCGM decrease during vestibular compensation is found in the ipsilesional midbrain, audiovestibular and visual cortex, as well as the hippocampal formation. Relative rCGM increase appears bilaterally in the cerebellum, sensorimotor, retrosplenial and parietal cortex. BL: baseline, D: day.

somatosensory, auditory, olfactory) networks within and between hemispheres increased from day 1 to 3 post UL and remained above baseline level up to day 15 post UL. The same tendency was seen for motor-executive networks. Limbic networks showed only a moderate change of metabolic connectivity during the course of vestibular compensation.

Dedicated analysis of connectivity of motor cortices revealed the following changes over time: Connections between hemispheres increased until day 3 post UL, especially those involving prefrontal, orbitofrontal and somatosensory cortices. Furthermore, intrahemispherical connections from the cingulate, prefrontal, orbitofrontal, somatosensory and parietal association cortex to the motor cortex increased preferentially in the right hemisphere until day 3 post UL. Thereafter, connections to the motor cortex went back to baseline level until day 15 post UL (Fig. 7).

Graph theoretical analysis of metabolic connections

Fifty-seven brain regions were used to create individual graphs according to the connections determined by Pearson's correlations. The number of graphs varied, with 37 disconnected graphs with at most 8 brain regions at the baseline, 19 graphs with at most 38 brain regions on day 1 post UL, 16 graphs with at most 41 brain regions on day 3 post UL, 31 graphs with at most 16 brain regions on day 7 post UL, and 27 graphs with at most 17 regions on day 15 post UL. For each day, the center and the rich club of the largest graph were determined, the latter by applying the highest available degree threshold. The determined brain regions are shown in Table 1.

Discussion

The current study analyzed short-term dynamic changes in the connectivity of individual brain regions and networks following unilateral peripheral vestibular damage in rats by statistical and graph theoretical analysis. The main findings were the following: 1) Functional brain networks exhibited a rapid reorganization during vestibular compensation, which paralleled the course of behavioral recovery. 2) In the vestibular network, ascending and crossing connections at various levels (brainstem, cerebellar, midbrain, thalamocortical) were recruited, thus including contralesional vestibular input for substitution of ipsilesional vestibular deficit. 3) During the peak of symptoms (day 3 post UL), vestibular, multisensory, and motor networks became maximally connected in large ensembles mostly by recruitment of interhemispheric and contralesional projections. 4) These connections between subnetworks were transient and gradually disappeared within the following days. 5) From a methodological perspective, serial analysis of the metabolic connectome by graph theory is a feasible method to depict dynamic whole-brain network arrangement after acute vestibular damage.

Changes of rCGM in individual brain regions during vestibular compensation

The central vestibular network is organized like a bilateral rope ladder system, which consists of crossed and uncrossed connections of strategic hubs (including the vestibular nuclei, vestibulocerebellum, midbrain, dorsolateral/anterior thalamic nuclei, and posterior in-

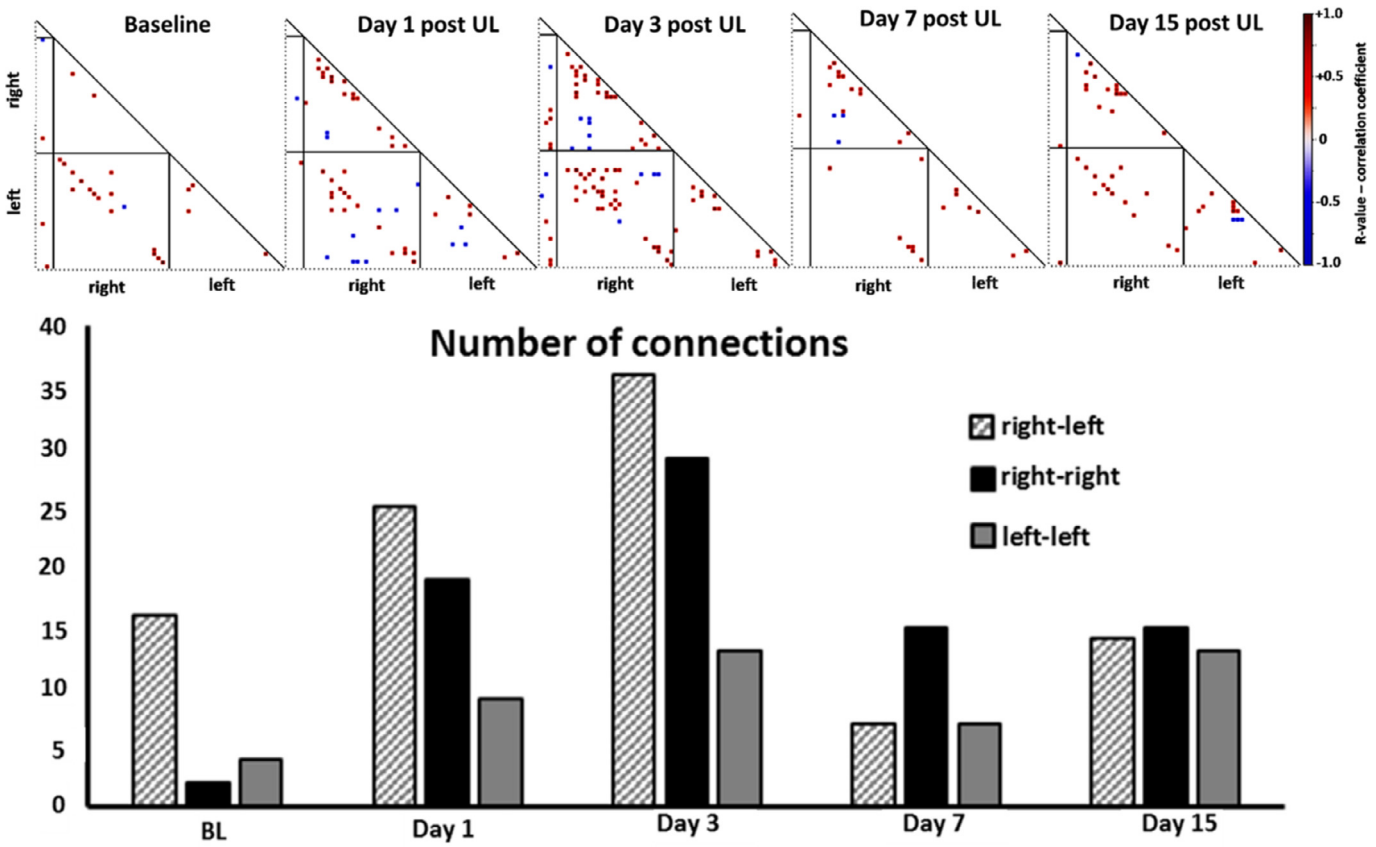

Fig. 5. Correlation matrices and number of correlations. Significant positive (red) and negative correlations (blue) ($|r| > 0.5$ and $p < 0.001$) are depicted in the correlation matrix for baseline and days 1, 3, 7, and 15 post UL. The total number of significant correlations between hemispheres (right-left) and within the contralesional (right) and the ipsilesional (left) hemispheres are shown in the bar plot. BL: baseline, UL: unilateral labyrinthectomy.

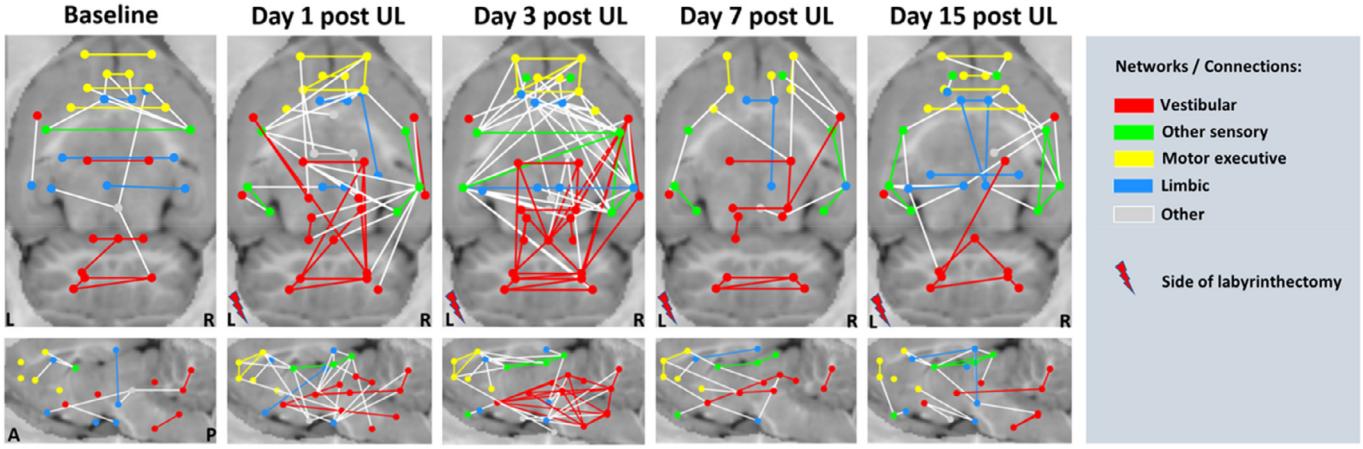

Fig. 6. Changes in metabolic connectivity of functional cerebral networks after unilateral labyrinthectomy. Significant metabolic connections are projected on to 2D planes of a 3D MRI cryoatlas and color-coded based on their relation to functional networks. Connections of hubs (depicted as dots) within a functional network are coded in the color of the network (vestibular networks: red; other sensory networks: green; motor executive networks: yellow; limbic networks: blue), while connections of hubs, which belong to different functional networks are drawn in white. A: anterior, L: left, P: posterior, R: right, UL: unilateral labyrinthectomy.

ferior vestibular cortex) (Brandt and Dieterich, 2017; Dieterich and Brandt, 1993; Kirsch et al., 2016; Zwergal et al., 2008; Zwergal et al., 2009). The bilateral structure is essential to establishing a balance of vestibular reflex arcs, as well as a global percept of verticality, self-motion, and spatial orientation (Brandt et al., 2014; Dieterich and Brandt, 2018). The vestibular network interacts closely with other sensory networks, e.g., in self-motion perception, orientation, postural and locomotor control and adaptation (Cullen, 2019; Zwergal et al., 2012).

A recent fMRI study in the rat indicated a bilateral activation of sensory cortices and associated thalamic nuclei after unilateral electrical stimulation of the medial vestibular nucleus (MVN). It further caused a synergistic activation of vestibular, visual, and auditory cortices ipsilateral to the MVN stimulation, when visual or auditory stimulation was applied in association (Leong et al., 2019). In general, ascending vestibular projections are dominant for the ipsilateral side of stimulation and the non-dominant hemisphere in humans (Dieterich et al., 2003; Dieterich et al.,

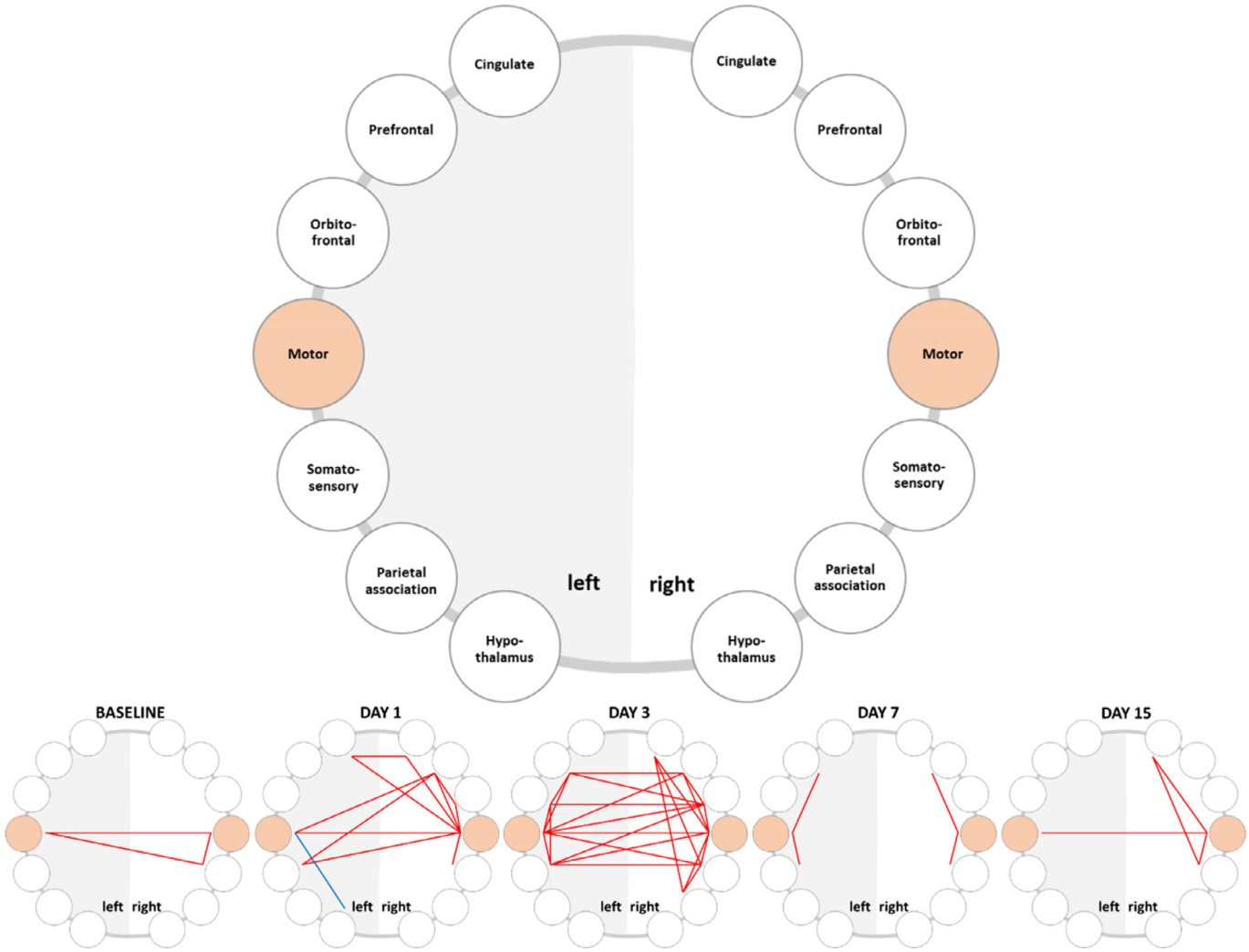

Fig. 7. Dynamic connectivity of motor cortices after unilateral labyrinthectomy. All significant metabolic connections of motor cortices are displayed in a reduced scheme of participating brain regions (upper graph). Connective involvement of the motor cortex increases until day 3 with an emphasis on interhemispherical and right intrahemispherical connections (lower graph). Positive correlations are depicted in red, negative correlations in blue.

2017). In rats, the left hemisphere seems to be dominant for vestibular processing (Best et al., 2014; Reuss et al., 2020). Complex vestibular pathways project to the hippocampal formation (including the entorhinal cortex, dentate gyrus) (Hitier et al., 2014). However, it is still unclear, if the ipsilateral dominance of vestibular projections in humans and rodents applies also for limbic projections. Our data support the view of an associated dominance of the ipsilateral ascending vestibular brainstem pathway to the limbic system and hippocampal formation. In earlier experiments, further functional connections have been demonstrated between the vestibular system and higher-order cortices (cingulate, retrosplenial, parietal), where head-direction cells are located and receive input from the inner ear (Leong et al., 2019; Yoder and Taube, 2014).

Acute unilateral peripheral vestibular lesions in humans have profound consequences on central vestibular processing at various brain levels (Brandt and Dieterich, 2017). In univariate analysis, the current rat study indicated an ipsilesional decrease and a contralesional increase of rCGM in vestibular 'core' hubs (including the midbrain, thalamus, and insular cortex), which persisted until day 15 post UL (Fig. 4). This study reproduced previous findings regarding vestibular compensation in an extended cohort (Lindner et al., 2017; Lindner et al., 2019; Zwergal et al., 2016). Our results are in accordance with the dominance of ipsilateral ascending vestibular projections in rats and humans (Best et al., 2014; Dieterich et al., 2003). Activation of the contralesional vestibular cortex was found also in patients with vestibular neuritis in the acute stage (Becker-Bense et al., 2014; Bense et al., 2004). In our study, an rCGM increase was found bilaterally in the cerebellum, which is known to contribute to the early stages of vestibular compensation (Beraneck et al., 2008; Darlington and Smith, 2000; Kitahara et al., 1997; Zwergal et al., 2016). Similarly, patients with a unilateral strategic medullary vestibular lesion showed bilateral cerebellar activation (Becker-Bense et al., 2013). Furthermore, the current study shows an rCGM increase in bilateral multisensory cortices (except some minor rCGM in the ipsilesional visual cortex) (Fig. 4) during vestibular compensation. Recruitment of visual, somatosensory, and auditory cortices can be interpreted as an attempt at sensory substitution (Green and Angelaki, 2010; Sadeghi et al., 2012). As mentioned above, the hippocampal formation in our study followed the principle of ipsilesional deactivation and contralesional activation, which could be taken as an indirect sign of a dominance of ipsilateral projections to the hippocampus in the rat (Fig. 4). As anxiety-related networks are concerned, rCMG increased significantly on days 1 and 3 in the right amygdala, while it remained unchanged or mildly decreased from day 1 to 15 in the left amygdala. Given that the right amygdala previously was associated with the processing of negative emotions such as fear or sadness (in contrast to both positive and negative emotions in the left amygdala) (Lanteaume et al.,

Table 1
Graph theoretical analysis of independent networks, centers, and rich-club brain regions in greatest networks during vestibular compensation.

	Number of **independent networks**	in the **greatest network** (highest number of connected brain regions)		
		Brain regions	*Centers*	*Rich-club*
BL	37	8	Cingulate cortex left	Cingulate cortex right Medial prefrontal cortex left Somatosensory cortex right Cingulate cortex left
D1	19	38	CortexParA right Somatosensory cortex right	Entorhinal cortex right Frontal association cortex right Motor cortex right Cerebellum white matter right
D3	16	41	Central canal and periaqueductal gray Posterior hippocampus left	Pons Cingulate cortex right Insular cortex right Motor cortex right Somatosensory cortex right Visual cortex right Vestibular nucleus right Motor cortex left Cingulate cortex left
D7	31	16	Frontal association cortex right	Frontal association cortex right Insular cortex right Colliculus superior right Thalamus right
D15	27	17	Posterior hippocampus left Somatosensory cortex left Retrosplenial cortex left CortexParA left	Cingulate cortex right Posterior hippocampus left Visual cortex left Somatosensory cortex left Retrosplenial cortex left CortexParA left Motor cortex right CortexParA right Somatosensory cortex right Retrosplenial cortex right Visual cortex right Cingulate cortex left

2007), this pattern likely indicates an amygdala-associated anxiety response to the aversive feeling of acute vestibular syndrome. rCGM in the right amygdala returned to almost normal in the process of successful vestibular compensation. Interestingly, in metabolic connectivity analysis the amygdala had no connections to any other brain region throughout the experiment. Successfully compensated acute unilateral vestibulopathy likely does not induce a structural change in anxiety-related networks.

Rearrangement of functional networks during vestibular compensation

The novel approach of this study is to depict not only relative changes of rCGM in individual brain regions, but rather dynamic changes of functional networks over time and in correlation with behavioral recovery during the course of vestibular compensation. The results indicate some general principles of network rearrangement after a peripheral vestibular lesion:

Firstly, functional brain networks become globally connected during the early stage of vestibular compensation by crossing, as well as up- and downstreaming pathways. Graph theoretical analysis indicated that, before UL, the brain consisted of a high number of disconnected clusters of brain regions each set up from a low number of connected brain regions. Until day 3 post UL, the number of separated clusters and disconnected brain networks subsequently decreased and one dominant cluster developed, which connected a majority of all brain regions in both hemispheres (Table 1). Within this cluster, the graph theoretical rich-club of regions included core vestibular, multisensory, and motor hubs. During the subsequent course, with improving symptoms the hub regions decreased their degree of connectivity. The dynamic of global network organization therefore reflects the initial and the subsequent functional and structural restoration of the vestibular tone imbalance.

Secondly, analysis of Pearson's correlations indicated a strong but transient recruitment specifically of vestibular connections after UL. While at baseline vestibular projections were mostly organized in local brainstem-cerebellar networks, the vestibular network started to connect ascending projections (mostly to the contralesional side at different brainstem levels) during the evolution of symptoms (days 1 and 3 post UL) (Fig. 6). Thereby, thalamo-cortical networks were

preferentially recruited. Following successful behavioral compensation until day 15 post UL, the vestibular connections shifted back to a more "reflexive" brainstem-cerebellar network. Multisensory (i.e., visual, somatosensory, auditory, and olfactory) regions started to become closely connected to each other and the vestibular system in both hemispheres during early vestibular compensation (Fig. 6). An increased connection of sensory systems persisted until day 15 post UL, which may be a sign of novel cortical representation of multisensory inputs (Becker-Bense et al., 2014). Accordingly, human MRI studies have shown a volume increase in bilateral somatosensory and visual cortical areas following acute vestibular unilateral vestibular loss (Helmchen et al., 2011; Lacour et al., 2016). This process is interesting from a clinical perspective, because some patients start to become more visually dependent after a unilateral peripheral vestibular lesion (Cousins et al., 2014; Roberts et al., 2018).

Thirdly, cortical motor and executive networks (including the prefrontal, orbitofrontal and cingulate cortex) were recruited with a maximum at day 3 post UL and preferentially in the right hemisphere (Fig. 7). In accordance, the right motor cortex appeared in the rich club on days 1, 3, 15 and the left motor cortex on day 3 post UL. These data suggest a prominent role of motor control during vestibular compensation. The relative asymmetry of motor cortex connectivity in favor of the contralesional right hemisphere could be interpreted as an active attempt to antagonize the falling tendency to the lesion side (left), which is driven by asymmetric vestibular-spinal inputs. Thereby, the recruitment of cortical motor networks possibly represents a top-down strategy to recover the motor components (i.e., postural asymmetry, mobility) of vestibular imbalance. The synchronicity of motor network degrees (Fig. 7) and motor behavior (Fig. 3) in the course of vestibular compensation underlines this hypothesis. The current study reinforces principles of physical balance treatment that are empirically established in clinical practice after acute unilateral vestibulopathy (Hall et al., 2016). Early therapeutic intervention is needed, given that the peak of connectivity changes in motor networks appears already by day 3 after the lesion. Active sensorimotor exercises in motion are relevant to foster the involvement of motor executive and multisensory networks during cortical network reorganization.

Methodological considerations, strengths and limitations

The current analysis aimed to investigate interactions of individual brain regions and network structures on a whole-brain level after UL. Therefore, Pearson's correlation and graph theory were used to characterize brain connectivity in the early phase of vestibular compensation. The fundamental assumption in our population-based approach was that regions with sufficiently correlating activity patterns within a cohort are connected. Due to the statistical nature of Pearson's correlation, the significance of detecting connections between individual brain regions improves with the increasing number of subjects used for analysis. In our case, the thresholds applied to the correlation results ensured that the informative value remained at a high level. So far, *in vivo* PET-based approaches to brain connectivity have been mostly applied in cross-sectional studies to investigate alterations of the metabolic connectome in different cohorts (Yakushev et al., 2017). Here, a preclinical cohort was analyzed with a highly standardized protocol, whose temporal resolution and reproducibility surpasses the feasibility of clinical imaging. This study shows that the procedure is suitable to analyze changes of the connectome longitudinally over time with a high sensitivity and therefore can be used to depict whole-brain changes and mechanisms of adaptive brain plasticity following damage to the peripheral or central nervous system in a short-term manner. The data of our study are in accordance with results derived from other methodological approaches in the past, which used fMRI (in combination with optogenetics or electrophysiology) to map whole-brain effects of peripheral or central vestibular stimulation (Leong et al., 2019; Rancz et al., 2015). These studies also showed activation of a wide-spread network of cortical (e.g., motor, sensory, high-order cortices) and subcortical (thalamus, brainstem, cerebellum) regions, which are engaged in vestibular processing. A methodological difference to fMRI experiments seems to be that animals are allowed to move freely after injection of [^{18}F]-FDG and before PET acquisition, which allows for active motor control and real multisensory feedback. Therefore, the motor and executive network changes were more pronounced in the current study compared to previous MRI studies (Rancz et al., 2015).

Potential limitations of our approach could be the spatial accuracy of segmentation procedures. Electrophysiological and optogenetic methods do have a higher space and time resolution. Furthermore, although the animals are awake during the PET examinations, a possible influence of repetitive anesthesia on the course of vestibular compensation cannot be excluded. Lastly, as the current UL rat model induces a combined peripheral audio-vestibular damage, the impact of hearing loss on brain network rearrangement cannot be separated from plasticity processes driven by peripheral vestibular failure completely.

Conclusion

This *in vivo* study in a rat model of unilateral labyrinthectomy reinforces the view that vestibular compensation is a highly dynamic process, which involves multiple functional networks at cortical and subcortical levels to achieve successful behavioral recovery. General principles seem to be an activation of ascending vestibular projections mostly on the contralesional side, a recruitment of bilateral multisensory (vestibular, visual, somatosensory, auditory, olfactory) and motor-executive networks to a large functional ensemble – potentially indicating functional substitution of vestibular loss - and a recalibration and reorganization of brainstem, cerebellar and thalamocortical multisensory networks during the course of successful vestibular compensation. This study demonstrates that statistical and graph theoretical approaches to identify the cerebral connectome are able to capture short-term variations associated with sensory disruptions in the rat and can provide a new understanding of brain plasticity during early vestibular compensation.

Credit author statement

Maximilian Grosch: Conceptualization, Methodology, Software, Validation, Formal analysis, Data Curation, Writing – Original Draft, Visualization **Magdalena Lindner:** Investigation, Project administration **Peter Bartenstein:** Resources, Writing – Review & Editing **Thomas Brandt:** Writing – Review & Editing **Marianne Dieterich:** Writing – Review & Editing **Sibylle Ziegler:** Resources, Writing – Review & Editing, Supervision **Andreas Zwergal:** Conceptualization, Resources, Writing – Original Draft, Visualization, Supervision, Project administration, Funding acquisition

Funding

The study was performed as a project of the German Center for Vertigo and Balance Disorders (DSGZ) with the support of the German Federal Ministry of Education and Research (BMBF) (grant number 01 EO 1401), the Deutsche Stiftung Neurologie (DSN) and the Hertie Foundation (to TB).

Declaration of Competing Interest

None.

Acknowledgments

The authors would like to thank the preclinical imaging team of the Nuclear Medicine Department of the LMU for their consistent commitment to the imaging tasks and their excellent documentation of the experiments. We thank Katie Göttlinger for copyediting the manuscript and Astrid Gosewisch for valuable comments.

Supplementary materials

Supplementary material associated with this article can be found, in the online version, at doi:10.1016/j.neuroimage.2020.117588.

References

Anniko, M., Wersall, J., 1977. Experimentally (atoxyl) induced ampullar degeneration and damage to the maculae utriculi. Acta Otolaryngol. 83, 429–440.

Beck, R., Gunther, L., Xiong, G., Potschka, H., Boning, G., Bartenstein, P., Brandt, T., Jahn, K., Dieterich, M., Strupp, M., la Fougere, C., Zwergal, A., 2014. The mixed blessing of treating symptoms in acute vestibular failure–evidence from a 4-aminopyridine experiment. Exp. Neurol. 261, 638–645.

Becker-Bense, S., Buchholz, H.G., Best, C., Schreckenberger, M., Bartenstein, P., Dieterich, M., 2013. Vestibular compensation in acute unilateral medullary infarction: FDG-PET study. Neurology 80, 1103–1109.

Becker-Bense, S., Dieterich, M., Buchholz, H.G., Bartenstein, P., Schreckenberger, M., Brandt, T., 2014. The differential effects of acute right- vs. left-sided vestibular failure on brain metabolism. Brain Struct. Funct. 219, 1355–1367.

Bense, S., Bartenstein, P., Lochmann, M., Schlindwein, P., Brandt, T., Dieterich, M., 2004. Metabolic changes in vestibular and visual cortices in acute vestibular neuritis. Ann. Neurol. 56, 624–630.

Beraneck, M., Hachemaoui, M., Idoux, E., Ris, L., Uno, A., Godaux, E., Vidal, P.P., Moore, L.E., Vibert, N., 2003. Long-term plasticity of ipsilesional medial vestibular nucleus neurons after unilateral labyrinthectomy. J. Neurophysiol. 90, 184–203.

Beraneck, M., McKee, J.L., Aleisa, M., Cullen, K.E., 2008. Asymmetric recovery in cerebellar-deficient mice following unilateral labyrinthectomy. J. Neurophysiol. 100, 945–958.

Bergquist, F., Ludwig, M., Dutia, M.B., 2008. Role of the commissural inhibitory system in vestibular compensation in the rat. J. Physiol. 586, 4441–4452.

Best, C., Lange, E., Buchholz, H.G., Schreckenberger, M., Reuss, S., Dieterich, M., 2014. Left hemispheric dominance of vestibular processing indicates lateralization of cortical functions in rats. Brain Struct. Funct. 219, 2141–2158.

Brandt, T., Dieterich, M., 2017. The dizzy patient: don't forget disorders of the central vestibular system. Nat. Rev. Neurol. 13, 352–362.

Brandt, T., Strupp, M., Dieterich, M., 2014. Towards a concept of disorders of "higher vestibular function". Front. Integr. Neurosci. 8, 47.

Cameron, S.A., Dutia, M.B., 1997. Cellular basis of vestibular compensation: changes in intrinsic excitability of MVN neurones. Neuroreport 8, 2595–2599.

Cousins, S., Cutfield, N.J., Kaski, D., Palla, A., Seemungal, B.M., Golding, J.F., Staab, J.P., Bronstein, A.M., 2014. Visual dependency and dizziness after vestibular neuritis. PLoS One 9, e105426.

Cullen, K.E., 2019. Vestibular processing during natural self-motion: implications for perception and action. Nat. Rev. Neurosci. 20, 346–363.

Curthoys, I.S., Halmagyi, G.M., 1995. Vestibular compensation: a review of the oculomotor, neural, and clinical consequences of unilateral vestibular loss. J. Vestib. Res. 5, 67–107.

Darlington, C.L., Smith, P.F., 2000. Molecular mechanisms of recovery from vestibular damage in mammals: recent advances. Prog. Neurobiol. 62, 313–325.

de Waele, C., Muhlethaler, M., Vidal, P.P., 1995. Neurochemistry of the central vestibular pathways. Brain Res. Brain Res. Rev. 20, 24–46.

Dieringer, N., 1995. 'Vestibular compensation': neural plasticity and its relations to functional recovery after labyrinthine lesions in frogs and other vertebrates. Prog. Neurobiol. 46, 97–129.

Dieterich, M., Bense, S., Lutz, S., Drzezga, A., Stephan, T., Bartenstein, P., Brandt, T., 2003. Dominance for vestibular cortical function in the non-dominant hemisphere. Cereb. Cortex 13, 994–1007.

Dieterich, M., Brandt, T., 1993. Ocular torsion and tilt of subjective visual vertical are sensitive brainstem signs. Ann. Neurol. 33, 292–299.

Dieterich, M., Brandt, T., 2018. Global orientation in space and the lateralization of brain functions. Curr. Opin. Neurol. 31, 96–104.

Dieterich, M., Kirsch, V., Brandt, T., 2017. Right-sided dominance of the bilateral vestibular system in the upper brainstem and thalamus. J. Neurol. 264, 55–62.

Dutheil, S., Brezun, J.M., Leonard, J., Lacour, M., Tighilet, B., 2009. Neurogenesis and astrogenesis contribution to recovery of vestibular functions in the adult cat following unilateral vestibular neurectomy: cellular and behavioral evidence. Neuroscience 164, 1444–1456.

Dutia, M.B., 2010. Mechanisms of vestibular compensation: recent advances. Curr. Opin. Otolaryngol. Head Neck Surg. 18, 420–424.

Green, A.M., Angelaki, D.E., 2010. Multisensory integration: resolving sensory ambiguities to build novel representations. Curr. Opin. Neurobiol. 20, 353–360.

Griffa, A., Van den Heuvel, M.P., 2018. Rich-club neurocircuitry: function, evolution, and vulnerability. Dialogues Clin. Neurosci. 20, 121–132.

S Hagberg, A., Swart, P., Chult, D., 2008. Exploring Network Structure, Dynamics, and Function using NetworkX Los Alamos National Lab.(LANL), Los Alamos, NMUnited States.

Hall, C.D., Herdman, S.J., Whitney, S.L., Cass, S.P., Clendaniel, R.A., Fife, T.D., Furman, J.M., Getchius, T.S., Goebel, J.A., Shepard, N.T., Woodhouse, S.N., 2016. Vestibular rehabilitation for peripheral vestibular hypofunction: an evidence-based clinical practice guideline: from the American physical therapy association neurology section. J. Neurol. Phys. Ther. 40, 124–155.

Helmchen, C., Klinkenstein, J.C., Kruger, A., Gliemroth, J., Mohr, C., Sander, T., 2011. Structural brain changes following peripheral vestibulo-cochlear lesion may indicate multisensory compensation. J. Neurol. Neurosurg. Psychiatry 82, 309–316.

Hitier, M., Besnard, S., Smith, P.F., 2014. Vestibular pathways involved in cognition. Front. Integr. Neurosci. 8, 59.

Kaufman, G.D., Anderson, J.H., Beitz, A.J., 1992. Brainstem Fos expression following acute unilateral labyrinthectomy in the rat. Neuroreport 3, 829–832.

Kirsch, V., Keeser, D., Hergenroeder, T., Erat, O., Ertl-Wagner, B., Brandt, T., Dieterich, M., 2016. Structural and functional connectivity mapping of the vestibular circuitry from human brainstem to cortex. Brain Struct. Funct. 221, 1291–1308.

Kitahara, T., Takeda, N., Saika, T., Kubo, T., Kiyama, H., 1997. Role of the flocculus in the development of vestibular compensation: immunohistochemical studies with retrograde tracing and flocculectomy using Fos expression as a marker in the rat brainstem. Neuroscience 76, 571–580.

Lacour, M., Helmchen, C., Vidal, P.P., 2016. Vestibular compensation: the neuro-otologist's best friend. J. Neurol. 263 (Suppl 1), S54–S64.

Lanteaume, L., Khalfa, S., Regis, J., Marquis, P., Chauvel, P., Bartolomei, F., 2007. Emotion induction after direct intracerebral stimulations of human amygdala. Cereb. Cortex 17, 1307–1313.

Leong, A.T.L., Gu, Y., Chan, Y.S., Zheng, H., Dong, C.M., Chan, R.W., Wang, X., Liu, Y., Tan, L.H., Wu, E.X., 2019. Optogenetic fMRI interrogation of brain-wide central vestibular pathways. Proc. Natl. Acad. Sci. USA 116, 10122–10129.

Lim, R., Callister, R.J., Brichta, A.M., 2010. An increase in glycinergic quantal amplitude and frequency during early vestibular compensation in mouse. J. Neurophysiol. 103, 16–24.

Lindner, M., Eilles, E., Günther, L., Gosewisch, A., Vomacka, L., Xiong, G., Oos, R., Bartenstein, P., Beck, R., Zwergal, A., 2017. Betahistine improves vestibular compensation after unilateral labyrinthectomy: a [18F] FDG-μPET study in the rat. EANM 2017.

Lindner, M., Gosewisch, A., Eilles, E., Branner, C., Kramer, A., Oos, R., Wolf, E., Ziegler, S., Bartenstein, P., Brandt, T., Dieterich, M., Zwergal, A., 2019. Ginkgo biloba Extract EGb 761 improves vestibular compensation and modulates cerebral vestibular networks in the rat. Front. Neurol. 10, 147.

Magnusson, A.K., Ulfendahl, M., Tham, R., 2002. Early compensation of vestibulo-oculomotor symptoms after unilateral vestibular loss in rats is related to GABA(B) receptor function. Neuroscience 111, 625–634.

Rancz, E.A., Moya, J., Drawitsch, F., Brichta, A.M., Canals, S., Margrie, T.W., 2015. Widespread vestibular activation of the rodent cortex. J. Neurosci. 35, 5926–5934.

Rastoldo, G., Marouane, E., El Mahmoudi, N., Pericat, D., Bourdet, A., Timon-David, E., Dumas, O., Chabbert, C., Tighilet, B., 2020. Quantitative evaluation of a new postur-o-locomotor phenotype in a rodent model of acute unilateral vestibulopathy. Front. Neurol. 11, 505.

Reuss, S., Siebrecht, E., Stier, U., Buchholz, H.G., Bausbacher, N., Schabbach, N., Kronfeld, A., Dieterich, M., Schreckenberger, M., 2020. Modeling vestibular compensation: neural plasticity upon thalamic lesion. Front. Neurol. 11, 441.

Ris, L., de Waele, C., Serafin, M., Vidal, P.P., Godaux, E., 1995. Neuronal activity in the ipsilateral vestibular nucleus following unilateral labyrinthectomy in the alert guinea pig. J. Neurophysiol. 74, 2087–2099.

Roberts, R.E., Ahmad, H., Patel, M., Dima, D., Ibitoye, R., Sharif, M., Leech, R., Arshad, Q., Bronstein, A.M., 2018. An fMRI study of visuo-vestibular interactions following vestibular neuritis. Neuroimage Clin. 20, 1010–1017.

Sadeghi, S.G., Minor, L.B., Cullen, K.E., 2012. Neural correlates of sensory substitution in vestibular pathways following complete vestibular loss. J. Neurosci. 32, 14685–14695.

Sanabria-Diaz, G., Martinez-Montes, E., Melie-Garcia, L.Alzheimer's Disease Neuroimaging, I., 2013. Glucose metabolism during resting state reveals abnormal brain networks organization in the Alzheimer's disease and mild cognitive impairment. PLoS One 8, e68860.

Schiffer, W.K., Mirrione, M.M., Biegon, A., Alexoff, D.L., Patel, V., Dewey, S.L., 2006. Serial microPET measures of the metabolic reaction to a microdialysis probe implant. J. Neurosci. Methods 155, 272–284.

Shao, M., Reddaway, R., Hirsch, J.C., Peusner, K.D., 2012. Presynaptic GABA(B) receptors decrease neurotransmitter release in vestibular nuclei neurons during vestibular compensation. Neuroscience 223, 333–354.

Smith, P.F., Curthoys, I.S., 1988. Neuronal activity in the ipsilateral medial vestibular nucleus of the guinea pig following unilateral labyrinthectomy. Brain Res. 444, 308–319.

Straathof, M., Sinke, M.R., Dijkhuizen, R.M., Otte, W.M., 2019. A systematic review on the quantitative relationship between structural and functional network connectivity strength in mammalian brains. J. Cereb. Blood Flow Metab. 39, 189–209.

Straka, H., Vibert, N., Vidal, P.P., Moore, L.E., Dutia, M.B., 2005. Intrinsic membrane properties of vertebrate vestibular neurons: function, development and plasticity. Prog. Neurobiol. 76, 349–392.

Tighilet, B., Chabbert, C., 2019. Adult neurogenesis promotes balance recovery after vestibular loss. Prog. Neurobiol. 174, 28–35.

Van Griethuysen, J.J., Fedorov, A., Parmar, C., Hosny, A., Aucoin, N., Narayan, V., Beets–Tan, R.G., Fillion-Robin, J.-C., Pieper, S., Aerts, H.J., 2017. Computational radiomics system to decode the radiographic phenotype. Cancer Res. 77, e104–e107.

Vibert, N., Beraneck, M., Bantikyan, A., Vidal, P.P., 2000. Vestibular compensation modifies the sensitivity of vestibular neurones to inhibitory amino acids. Neuroreport 11, 1921–1927.

Vignaux, G., Chabbert, C., Gaboyard-Niay, S., Travo, C., Machado, M.L., Denise, P., Comoz, F., Hitier, M., Landemore, G., Philoxene, B., Besnard, S., 2012. Evaluation of the chemical model of vestibular lesions induced by arsanilate in rats. Toxicol. Appl. Pharmacol. 258, 61–71.

Yakushev, I., Drzezga, A., Habeck, C., 2017. Metabolic connectivity: methods and applications. Curr. Opin. Neurol. 30, 677–685.

Yamanaka, T., Him, A., Cameron, S.A., Dutia, M.B., 2000. Rapid compensatory changes in GABA receptor efficacy in rat vestibular neurones after unilateral labyrinthectomy. J. Physiol. 523 (Pt 2), 413–424.

Yoder, R.M., Taube, J.S., 2014. The vestibular contribution to the head direction signal and navigation. Front. Integr. Neurosci. 8, 32.

Zwergal, A., Buttner-Ennever, J., Brandt, T., Strupp, M., 2008. An ipsilateral vestibulothalamic tract adjacent to the medial lemniscus in humans. Brain 131, 2928–2935.

Zwergal, A., Gunther, L., Brendel, M., Beck, R., Lindner, S., Xiong, G., Eilles, E., Unterrainer, M., Albert, N.L., Becker-Bense, S., Brandt, T., Ziegler, S., la Fougere, C., Dieterich, M., Bartenstein, P., 2017. In vivo imaging of glial activation after unilateral labyrinthectomy in the rat: a [(18)F]GE180-PET study. Front. Neurol. 8, 665.

Zwergal, A., Linn, J., Xiong, G., Brandt, T., Strupp, M., Jahn, K., 2012. Aging of human supraspinal locomotor and postural control in fMRI. Neurobiol. Aging 33, 1073–1084.

Zwergal, A., Schlichtiger, J., Xiong, G., Beck, R., Gunther, L., Schniepp, R., Schoberl, F., Jahn, K., Brandt, T., Strupp, M., Bartenstein, P., Dieterich, M., Dutia, M.B., la Fougere, C., 2016. Sequential [(18)F]FDG microPET whole-brain imaging of central vestibular compensation: a model of differentiation-induced brain plasticity. Brain Struct. Funct. 221, 159–170.

Zwergal, A., Strupp, M., Brandt, T., Buttner-Ennever, J.A., 2009. Parallel ascending vestibular pathways: anatomical localization and functional specialization. Ann. NY Acad. Sci. 1164, 51–59.